


RESEARCH ARTICLE

# A variable stiffness design method for soft robotic fingers based on grasping force compensation and linearization

Xiaowei Shan, Litao Xu  and Xuefei Li

School of Mechanical-Electronic and Vehicle Engineering, Beijing University of Civil Engineering and Architecture, Beijing, China

**Corresponding author:** Xiaowei Shan; Email: [xiaowei.shan@mail.mcgill.ca](mailto:xiaowei.shan@mail.mcgill.ca)

**Received:** 7 September 2023; **Revised:** 8 March 2024; **Accepted:** 21 April 2024; **First published online:** 10 May 2024

**Keywords:** soft robotic finger; grasping performance; grasping force compensation; variable stiffness; finite element analysis; design methodology

## Abstract

Soft fingers play an increasingly important role in robotic grippers to achieve adaptive grasping with variable stiffness features. Previous studies of soft finger design have primarily focused on the optimization of the structural parameters of existing finger structures, but limited efforts have been put into the design methodology from fundamental grasping mechanisms to finger structures with desired grasping force features. To this aim, a fundamental architecture of soft fingers is proposed for analyzing common soft finger features and the influence of the internal structures on the overall grasping performance. In addition, three general performance metrics are introduced to evaluate the grasping performance of soft finger designs. Then, a novel method is proposed to combine the variable stiffness structure with the fundamental architecture to compensate for the grasping force of the finger and linearization. Subsequently, an embodiment design is proposed with a cantilever spring-based variable stiffness (CSVS) mechanism based on the method, and a multi-objective optimization method is employed to optimize the design. Besides, the CSVS features are analyzed through finite element analysis (FEA), and by comparing the grasping performance between the V-shape finger and the CSVS finger, it is demonstrated that the design method can effectively shorten the pre-grasp stage and linearize the grasping force in the post-grasp stage while reducing the likelihood of sliding friction between the finger and the grasped object. Finally, experiments are conducted to validate the accuracy of the FEA model, the effectiveness of the design methodology, and the adaptability of the CSVS finger.

## 1. Introduction

Robotic grippers play a pivotal role in modern automation, and the variability of objects that a robot or automated machine needs to grasp has led gripper manufacturers to design different types of grippers to accommodate this issue [1, 2]. The soft robotic gripper is primarily employed for the manipulation of delicate and deformable objects in unstructured environments [3–5]. In comparison to conventional rigid grippers, soft robotic grippers offer superior flexibility, convenient control, and versatile applicability [6]. Soft robotic hands can be classified according to the driving principles [7–15]. Among them, soft grippers based on passive adaptive structures rely on contact with objects to trigger the deformation of the gripper structure, thus achieving grasping. Compared to other types, they have simpler driving and control mechanisms, so they can be easily installed on existing industrial actuators, thereby transforming traditional rigid industrial robots into hybrid stiffness robots with certain softness characteristics [6].

Due to the inherent nature of the flexible and deformable materials of the soft robotic grippers, they often encounter issues of unstable grasping and difficulty in controlling the grasping force. Addressing these issues, the bistable adaptive fingers designed in refs. [15, 16] can adopt two grasping modes to achieve stable grasping for different objects. The adaptive grippers obtained through topology optimization as described in refs. [17, 18] are capable of delivering constant grasping force. The shape-adaptive

fingers with variable stiffness designed in refs. [19] and [20] not only enhance finger rigidity but also enable flexible grasping of more complex and delicate objects.

For the design optimization of finger structures, most designs have been inspired by sudden insights or the optimization of existing representative structures, such as the Fin Ray Effect (FRE) finger [13]. Moreover, current research on FRE fingers primarily focuses on improving grasping performance through mathematical modeling [21, 22] or optimizing the internal structure, such as altering the thickness, shape, inclination angle, and spacing of the crossbeams [3, 23–28]. However, there is a lack of research exploring how to design the internal structure of soft fingers based on prescribed grasping characteristics without relying on sudden insights or existing structures.

When designing well-functioning fingers, it is crucial to consider performance as a key criterion in the early stages of the mechanical design process [29]. Performance evaluation metrics for fully actuated hands and underactuated hands are detailed in references [30] and [31], respectively. However, there is currently no clear definition of grasping performance for soft fingers in the existing literature. Some works evaluate the adaptability of the fingers only often based on their deformation displacement, such as the maximum displacement [10], the total displacement at the fingertip [13], the fingertip displacement in the  $X$  and  $Y$  directions on the bending plane [3, 28], and a combination of the fingertip and contact point displacements [32]. Other works assess the finger's load capacity through the maximum grasping force [23] and maximum grasping mass [24]. However, these evaluation metrics only consider the finger's adaptive capability based on its enveloping shape or assess its load-bearing capacity based on the final grasping state, without considering the actual distribution of contact area, variations in grasping force magnitude, or changes in grasping force direction during finger deformation. Indeed, these metrics are closely related to whether the finger can successfully stably accomplish the grasping task.

In this work, we first propose three performance evaluation metrics for assessing the grasping performance of soft finger grippers, which are used to evaluate the design of soft fingers. Then, starting from the grasping characteristics of the fundamental architecture of the A-shape, utilizing the variable stiffness property of the cantilever spring structure to compensate for the grasping force and obtaining a variable stiffness finger. Finally, the effectiveness of the grasping force compensation method is validated through FEA and real experiments. This work aims to propose an innovative design methodology to compensate for the desired grasping characteristics by designing the internal structure of soft fingers with variable stiffness features.

## 2. Fundamental architecture and performance metrics

### 2.1. Design of the fundamental architecture

A fundamental architecture of the soft fingers provides an essential arrangement of components, while a structure provides a detailed arrangement within components on how they interact with each other, and what mechanism is used to achieve desired performance. When using a beam-type finger architecture to grasp an object, it is common to define the side of the finger that comes into contact with the grasped object as the front beam, while the opposite side is referred to as the back beam. The beam that serves to fix the finger is known as the bottom beam.

The FRE proposed by biologist Kniese is based on the principle that when a force is applied to one side of a fish fin, the fin will bend and deform in the opposite direction to the applied force. The fin's A-shape structure consists of two bones with connecting tissues in the form of crossbeams spaced between the tip and the base [33], which was later commercialized by Festo as a soft finger [5, 14], as shown in Fig. 1(a). The current research on the internal structure design of FRE fingers is based on retaining the most primitive symmetric structure and modifying the internal tissue structure of the fish fin. Even though the origins were biologically motivated, one should not rely totally on biological motivation. But instead, engineering principles are more expected to be relied on for building more effective structures. For example, in practical robotic hand operations, typically only one side

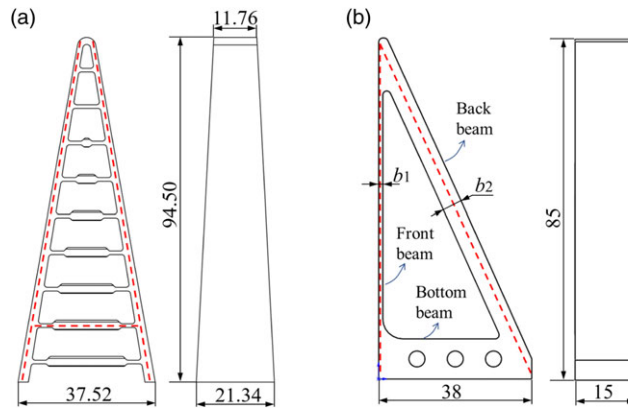


**Figure 1.** Fundamental architectures of soft fingers with beams (in mm): (a) A commercial Fin Ray Effect finger with the A-shape architecture: DHAS-80; (b) A design of the V-shape architecture.

of the finger is used for grasping. Therefore, this biological symmetry is not necessary in practical applications.

Considering that the A-shape architecture finger needs to be tilted at a certain angle to make the front beam perpendicular to the grasping direction when assembled on a parallel gripper, we propose a fundamental architecture of an asymmetric inverted V-shape, with a right-angle feature at the front and bottom beam, and apart from these supporting beams and the assembly of driving components, there are no other specific internal structures, as shown Fig. 1(b). Free from the symmetric constraint of the A-shape architecture, by setting apart the internal structure from the external structure, it facilitates the mechanism design of the internal structure as well as the analysis of the mechanical influence partially and as a whole. Based on the influence of the thickness values of the front and back beams on the grasping force [10, 21], Fig. 1(b) illustrates a finger design with a V-shaped architecture, where  $b_1$  and  $b_2$  represent the thickness of the front and back beams, respectively. The A-shape and V-shape features of the underlying architectures are indicated by the contour dotted lines in Figs. 1(a) and (b), respectively.

## 2.2. Simulation setting

A static structural analysis for the deformation of the V-shape soft fingers was created using ANSYS software. Figure 2 shows the two-finger grasping configuration grasping an object, while the simulation is only conducted on the right-side single finger and half cylinder based on the symmetric feature of the configuration to reduce the computational load. The grasping depth is defined as the relative displacement between the finger and the grasped object. The deformation of the finger at a grasping depth of 15 mm is shown on the right side of Fig. 2.

To fully demonstrate the adaptability of the finger and facilitate the analysis of the distribution of grasping force, a cylindrical object is to be grasped with a material of aluminum alloy and a diameter of 30 mm, referring to the test benchmark of National Institute of Standards and Technology [34]. Setting up frictional contact between the cylindrical object and the front beam of the finger, a friction coefficient of 0.15 is set [35]. A fixed constraint is applied to the bottom of the finger and a displacement of 15 mm is applied to the left side of the cylindrical object, while the movement of the cylindrical object in the direction of the  $y$ -axis and  $z$ -axis is prohibited. NinjaFlex material from Ninjatek is chosen for making soft fingers, a highly flexible thermoplastic polyurethane material with a Shore hardness of 85A and a wide range of application areas [3]. The classical two-parameter Mooney-Rivlin model is used to

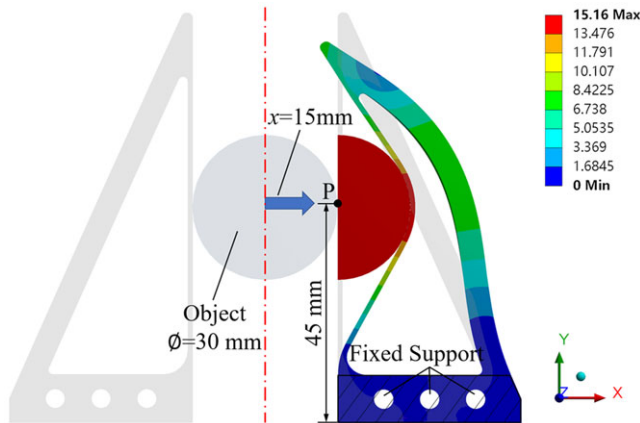


**Figure 2.** Illustration of an finite element analysis model of the two-finger configuration.

describe the mechanical properties of a soft finger using NinjaFlex material. The Mooney-Rivlin two-parameter model strain energy density function expression is given by:

$$\psi(I_1, I_2) = \frac{\mu_1}{2} (I_1 - 3) + \frac{\mu_2}{2} (I_2 - 3) \quad (1)$$

where  $\psi$  is the strain energy density;  $\mu_1 = 0.77$  and  $\mu_2 = 2.94$  are both material coefficients [36];  $I_1$  and  $I_2$  are the first and second invariant of deformation, respectively. By setting the  $\mu_1$  and  $\mu_2$  material coefficients in the ANSYS material library to define the NinjaFlex material properties, the Mooney-Rivlin model can be then used for the simulations of the fingers under study and provide a comparison with the physical experiment using the same material in Section 5.

### 2.3. Grasping performance metrics

To evaluate the performance of the soft fingers during grasping, three grasping performance metrics are proposed: the grasping force response  $W$ , and the grasping force angle  $\theta$ , the contact area ratio  $M$ . Additionally, to present the proposed grasping performance metrics more intuitively and accurately, the simulation results of the V-shaped finger are showcased in Section 2.4.

#### 2.3.1 Grasping force response

The grasping force response is defined as the variation of the grasping force with grasping depth during the grasping process of a soft finger. Figure 3 shows the preliminary result of the grasping force with respect to the grasping depth.

In Fig. 3(a), the inflection point of the grasping force response and the grasping force angle are determined using a numerical differentiation method, identifying the point where the curvature of the curve is maximum. The appearance of this inflection point is attributed to the superior adaptability of the front beam when the fingers initially make contact with the grasped object. At this stage, the front beam undergoes significant deformation to conform to the shape of the object, resulting in a relatively low grasping force. As the fingers adapt to the shape of the grasped object, an increased grasping depth induces greater deformation in the back beam. In this design, the stiffness of the back beam is relatively high, making its deformation the primary factor that influences the magnitude of the grasping force. Consequently, a significant increase in the grasping force occurs.

Based on the inflection point of the grasping force response, the grasping process can be divided into two stages: pre-grasp and post-grasp. During the process of grasping an object with soft fingers, it is crucial to maintain a relatively low grasping force in the initial pre-grasp stage to avoid excessive stress

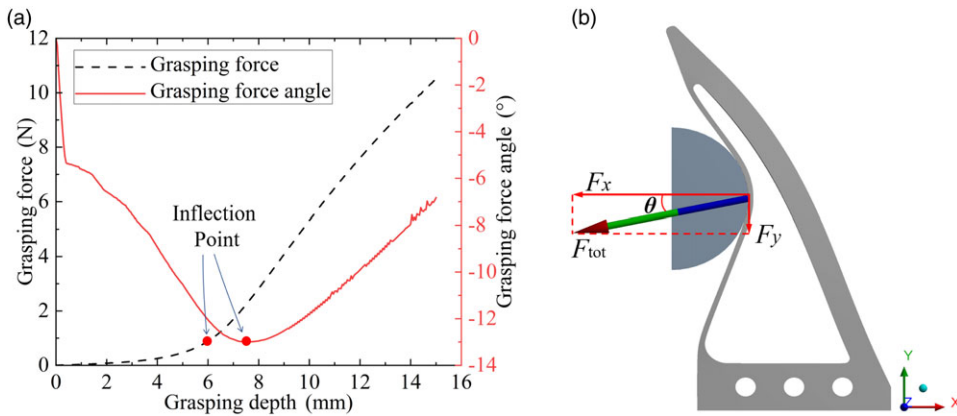


**Figure 3.** Illustration of the grasping force and angle: (a) The grasping force magnitude and angle with respect to the grasping depth; (b) The grasping force angle.

on the object. However, in the post-grasp stage, when the fingers have adapted to the shape of the object, a higher grasping force can be applied to enhance the finger’s load-bearing capacity. The expression of the grasping force response is as follows:

$$W(x) = \int_0^x F_{tot}(x) dx \tag{2}$$

Where  $x$  is the grasping depth,  $F_{tot}$  is the magnitude of the total grasping force at the grasping depth  $x$ ,  $W(x)$  is the grasping force response, and its specific meaning is the work done by the soft finger on the object during the grasping process at a certain external driving force and grasping depth. During the grasping process, the greater the work done by the fingers, the larger the deformation experienced by the fingers, and consequently, the greater the strain energy stored in the fingers.

### 2.3.2 Grasping force angle

The grasping force angle is defined as the angle between the direction of the total grasping force and the closing direction (negative  $x$ -axis) of the fingers. More intuitively in Fig. 3(b), the angle between  $F_{tot}$  and the  $x$ -axis is the grasping force angle. The values of the forces in the out-of-the-plane axis ( $F_z$ ) are in all cases well below a magnitude of  $10^{-2}$  N and are therefore negligible. The expression of the grasping force direction is defined by the angle:

$$\theta(x) = \arctan \frac{F_y(x)}{|F_x(x)|} \tag{3}$$

Where  $F_x(x)$  is the component of  $F_{tot}$  along the closing direction of the fingers;  $F_y(x)$  is the component of  $F_{tot}$  perpendicular to the closing direction of the fingers; and  $\theta(x)$  is the grasping force angle. The solid line in Fig. 3(a) shows the variation of the grasping force angle with the grasping depth. If  $\theta(x)$  is positive, the direction of the grasping force is biased toward the fingertip, and the object has the tendency to slide outward; if  $\theta(x)$  is negative, the direction of the grasping force is biased toward the bottom of the finger, and the object tends to slide inward. In the grasping process, the smaller the absolute value of the angle  $\theta(x)$ , the lower the likelihood of sliding occurrence, which leads to a more stable grasping state.

### 2.3.3 Contact area ratio

The shape, size, and characteristics of the grasped object can affect the contact area between the finger and the object during grasping. Therefore, the contact area ratio is defined as the ratio of the contact

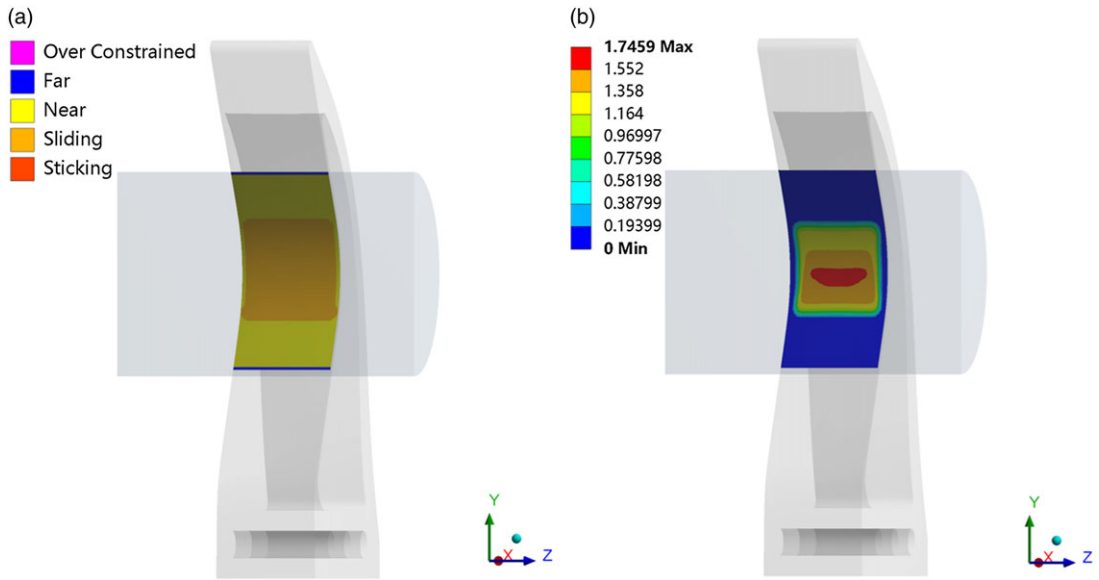


**Figure 4.** Example contact features of the front beam: (a) Contact status; (b) Sliding distance.

area between the finger and the grasped object to the area of the front beam of the finger. The expression is as follows:

$$M(x) = \frac{A_c(x)}{A_f} \tag{4}$$

Where  $A_c(x)$  is the contact area between the front beam of the finger and the grasped object at the grasping depth  $x$ ;  $A_f$  is the area of the front beam of the finger, and for fingers of the same architecture and size, it is a constant value; and  $M(x)$  is the contact area ratio. The larger the value of  $M(x)$  at the same grasping depth  $x$ , the larger the contact area, indicating better adaptability of the finger. To visualize the contact area ratio through an example FEA, the translucent dimetric view is shown in Fig. 4, where the contact feature between the front beam of the finger and the grasped object is on the finger’s side.

The color codes in Fig. 4(a) divide the status of the simulated contact into five types. “Far” and “Over constrained” means far away and no contact; “Near” means close but no contact; “Sliding” means contact with some tangential sliding; and “Sticking” means close contact without sliding. It should be noted that the “Near” status is around the magnitude of 0.5 mm ~ 1 mm, which can be visually unnoticeable and lead to the wrong conclusion of adaptivity. Figure 4(b) illustrates the sliding distance in the sliding status between the grasped object and the front beam of the finger. The main cause of such sliding is primarily the deformation of the fingers, leading to localized tensile deformation in the finger material and resulting in a change of the contact points of the finger. The sliding is inevitable for soft fingers and has a positive correlation with the grasp depth. However, this deformation is minimal. The maximum sliding distance of the contact point is only 1.75 mm. Nevertheless, since the contact surface is composed of numerous contact points with slight sliding motions, a sliding region of a certain area occurs during the grasping process, corresponding to the middle rectangular area in Fig. 4(a). Hence, the contact area includes the total area under both “Sliding” and “Sticking” statuses. The larger the contact area of the finger with the surface of the grasped object in the statuses of “Sliding” and “Sticking”, the finger better adapts to the surface of the object, resulting in a more stable grasp.

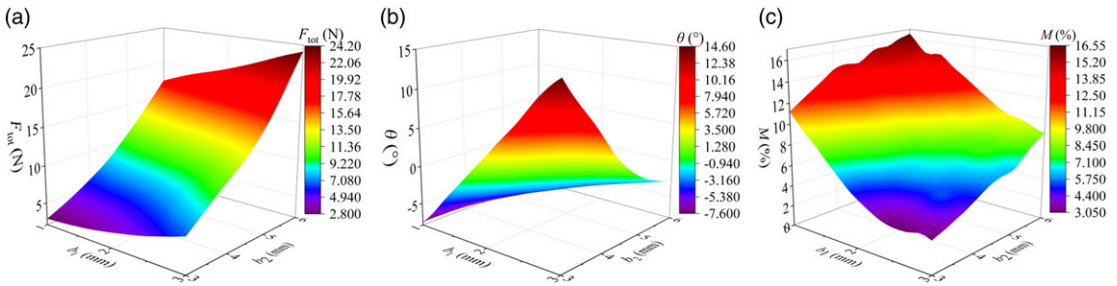


**Figure 5.** The response surface of the thicknesses of the front beam and back beam to the optimization objectives: (a) The front-beam thickness  $b_1$ , back-beam thickness  $b_2$ , and the grasping force  $F_{tot}$ ; (b) The front-beam thickness  $b_1$ , back-beam thickness  $b_2$ , and the grasping force angle  $\theta$ ; and (c) The front-beam thickness  $b_1$ , back-beam thickness  $b_2$ , and the contact area ratio  $M$ .

### 2.4. Optimization of the V-shape finger

The design variables are then grouped into a vector  $\mathbf{p}_1 = [b_1 \ b_2]^T$  for the optimization of the V-shape finger. The optimization objectives include the grasping force  $F_{tot}$  directly related to the variation in the grasping force response, the grasping force angle  $|\theta|$ , and the contact area ratio  $M$ . Therefore, the multi-objective optimization problem can be described in terms of the design variables:

$$\max [F_{tot}(\mathbf{p}_1), -|\theta(\mathbf{p}_1)|, M(\mathbf{p}_1)] \tag{5}$$

$$\text{subject to } \begin{cases} 1 \text{ mm} \leq b_1 \leq 3 \text{ mm} \\ 3 \text{ mm} \leq b_2 \leq 6 \text{ mm} \end{cases} \tag{6}$$

The selected method in the design of experiments (DOEs) is Latin hypercube sampling, and the optimization method utilized is the Multi-Objective Genetic Algorithm. The response surfaces of the thicknesses of the front beam ( $b_1$ ) and back beam ( $b_2$ ) to the optimization objectives are plotted in Fig. 5.

From Fig. 5(a), it can be observed that the grasping force response of the fingers is nearly proportional to the thickness of both the front and back beams of the fingers. Moreover, the influence of the back beam on the grasping force is greater than that of the front beam, indicating that the stiffness of the back beam is the primary factor affecting the grasping force of the fingers. From Fig. 5(b), it can be found that the grasping force angle increases with the increase in the front-beam thickness and decreases with the increase in the back-beam thickness. Moreover, the influence of the back beam on the angle diminishes gradually after reaching 5 mm. In Fig. 5(c), it is visualized that the contact area ratio decreases with the increase in the front-beam thickness and increases with the increase in back-beam thickness. Therefore, thinner front beams and thicker back beams contribute to better adaptability of the fingers. The final optimization result of design variables is  $\mathbf{p} = [1 \ 5]^T$ , which generates a grasping force of 10.50 N, a grasping force angle of  $-6.83^\circ$ , and a contact area ratio of 15.10%.

### 3. Design method of grasping force compensation

According to Fig. 5(c), one can observe that the thinner front beam gives the finger better adaptivity, but due to the finger does not reach the inflection point of the grasping force response until the grasping depth is 6 mm, it makes the pre-grasp stage of the finger over-represented, which will lead to the possible unstable grasping of the finger when grasping smaller objects; in the post-grasp stage, the grasping force varies nonlinearly with the grasping depth. In addition to this, a large change in the grasping force angle exists during the grasping process, with a maximum value of about  $-13^\circ$ , which will cause the object to slide toward the bottom of the finger under the force of finger grasping, and the sliding friction may cause damage to the surface vulnerable objects.

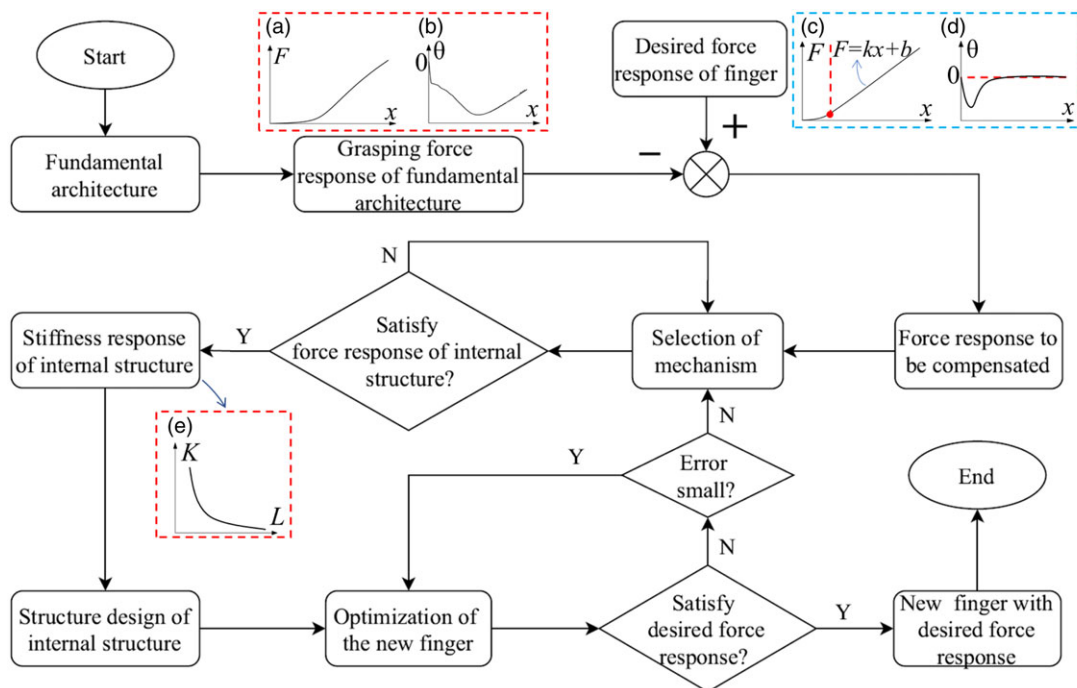


**Figure 6.** Flowchart of the design based on grasping force compensation: (a) and (b) Grasping force magnitude and angle of the fundamental structure; (c) and (d) The desired grasping force magnitude and angle of the finger; (e) Stiffness of the leaf spring.

To achieve the desired grasping performance characteristics of the finger, we propose a design method for the internal structure of the finger to achieve the desired grasping performance by compensating for the required grasping characteristics. Figure 6 shows the specific design methodology illustrated in the flowchart.

In this paper, we utilize this method to design an internal structure within the finger with variable stiffness characteristics as shown in Fig. 6(e) to compensate for the grasping force deficiency in the V-shape finger, thereby achieving the following desired grasping performance:

1. In the pre-grasp stage, it aims to reach the grasping force response inflection point earlier while ensuring the finger’s adaptability.
2. In the post-grasp stage, the grasping force should increase linearly with the grasping depth. This ensures that the finger can predictably provide sufficient grasping force to securely hold the object.
3. Throughout the grasping process, a stable grasping force angle should be maintained as close to zero as possible. This is done to minimize any sliding between the fingers and the object, thereby enhancing the overall stability of the grasping.

To achieve the desired grasping performance mentioned earlier, it is necessary to incorporate a variable stiffness internal structure to compensate for the inherent response lag and nonlinearity issues present in the finger force response curve. A variable stiffness mechanism refers to a type of mechanism that enables the adjustment of its stiffness based on the specific requirements of a task [37, 38]. Among them, the cantilever spring-based variable stiffness (CSVS) mechanism is typically achieved by altering the effective length of the leaf spring to achieve the variable stiffness characteristics [39]. The CSVS mechanism is incorporated by designing a cantilever spring within the V-shaped finger, forming a cantilever spring in terms of the elastic properties of the soft finger, as shown in Fig. 7.



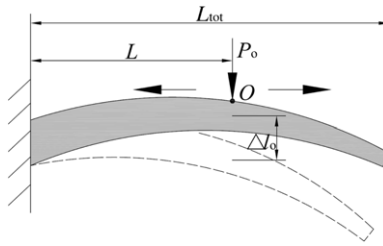


Figure 7. Design of the cantilever spring-based variable stiffness mechanism in the new finger.

In this diagram,  $L_{tot}$  represents the total length of the cantilever spring,  $L$  represents the effective length of the cantilever spring, point  $O$  is the contact point between the cantilever spring and the front beam,  $P_o$  is the force acting on the contact point  $O$  by the front beam, and  $\Delta l_0$  is the displacement of the cantilever spring at contact point  $O$  under the action of  $P_o$ .

The position of the contact point of this structure with the front beam also changes under different grasping depths, thereby altering the effective length of the cantilever spring. Additionally, the different cross-sectional areas of the cantilever spring also contribute to the variable stiffness characteristics of the structure.

According to the deflection equation of a cantilever beam, the stiffness can be expressed as:

$$K = \frac{3EI}{L^3} \tag{7}$$

Where  $L$  is the effective length of the cantilever spring,  $E$  is the modulus of elasticity of the cantilever spring, and  $I$  is the moment of inertia of the cross-section at the contact position between the cantilever spring and the front beam. From Equation (7), it follows that as the effective length decreases, the stiffness of the structure shows a nonlinear increase. The relationship between the stiffness and the effective length satisfies the feature in Fig. 6(e). Hence, a cantilever spring with variable stiffness is designed inside the finger, where its effective length decreases with the increase of grasping depth. It is expected to compensate for the grasping force and achieve a linear variation of grasping force with grasping depth in the post-grasp stage while ensuring stable grasping of the finger in the grasping process.

#### 4. Design and analysis of the CSVS finger

##### 4.1. Design and optimization of the CSVS finger

The new finger design based on the V-shape architecture in addition to the CSVS mechanism is denoted as the CSVS finger. The overall size of the new finger remains the same as that of the V-shape finger, but the difference is the cantilever spring structure added to the back beam. Fig. 8 shows the parameters and simulation settings for the CSVS finger.

A parameterized model of the CSVS finger is established in Fig. 8(a), where  $r$  is the bending radius of the cantilever spring,  $h$  is the height of the bottom end of the cantilever spring from the base of the finger,  $t_1$  is the thickness of the bottom end of the cantilever spring,  $t_2$  is the thickness of the top end of the cantilever spring, and  $a$  is the distance between the cantilever spring and the front beam. The design variables are then grouped into a vector  $\mathbf{p}_2 = [r \ h \ t_1 \ t_2 \ a]^T$  for the optimization of the CSVS finger. The optimization objectives include the grasping force  $F_{tot}$ , the grasping force angle  $|\theta|$ , and the contact area ratio  $M$ . Therefore, the multi-objective optimization problem can be described in the same way as in Eq. (5):

$$\max [F_{tot}(\mathbf{p}_2), -|\theta(\mathbf{p}_2)|, M(\mathbf{p}_2)] \tag{8}$$

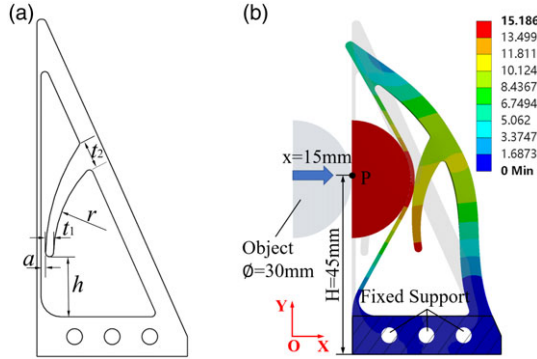


**Figure 8.** Parameters and simulation settings for the cantilever spring-based variable stiffness (CSVS) finger: (a) Parametric model of the CSVS finger; (b) Optimized simulation settings for the CSVS finger.

$$\text{subject to } \begin{cases} 50 \text{ mm} \leq r \leq 150 \text{ mm} \\ 15 \text{ mm} \leq h \leq 20 \text{ mm} \\ 1.5 \text{ mm} \leq t_1 \leq 3 \text{ mm} \\ 7 \text{ mm} \leq t_2 \leq 9 \text{ mm} \\ 1 \text{ mm} \leq a \leq 2 \text{ mm} \end{cases} \quad (9)$$

The simulation setup illustrated in Fig. 8(b) for the finger grasping is the same as described in Section 2.2. Most importantly, another frictional contact was introduced between the cantilever spring and the inner surface of the front beam. The DOEs and optimization method is the same as described in Section 2.4. The final optimization result of design variables is  $\mathbf{p} = [50.8 \ 15 \ 2 \ 8.5 \ 1.1]^T$ , which generates a grasping force of 11.21 N, a grasping force angle of  $-1.82^\circ$  and a contact area ratio of 13.48%.

**4.2. Analysis of the CSVS features**

To verify the variable stiffness characteristics of the CSVS mechanism, a simulation analysis is performed using the CSVS finger obtained from the optimization in Section 4.1. Fig. 9 shows the deformation of the CSVS fingers and the position of the contact surface between the front beam and the cantilever spring at different grasping depths.

From the deformation of the CSVS finger in Fig. 9, the position of contact between the cantilever spring and the front beam is a point and varies with the grasping depth. Thereby, a variable stiffness effect can be obtained by changing the effective lever of the cantilever spring. Based on Fig. 9(a), it can be observed that the contact between the front beam and the cantilever spring occurs at a grasping depth of 2.5 mm. Therefore, in this study, within the range of 2.5 mm to 15 mm grasping depth, data points are selected at intervals of 0.5 mm to calculate the effective length of the cantilever spring. Finally, based on Equation (7) in Section 3, the stiffness of the cantilever spring is calculated for different effective lengths.

Figure 10 shows the relationship between the grasping depth, the effective length of the cantilever spring, and the cantilever spring stiffness. From the variation of cantilever spring stiffness with effective length, it can be observed that the cantilever spring exhibits a nonlinear stiffness that gradually increases as the effective length decreases, similar to the trend shown in Fig. 6(e). This verifies that the designed cantilever spring possesses variable stiffness characteristics similar to the CSVS mechanism. From the variation of cantilever spring stiffness with grasping depth, it can be observed that the stiffness value of the cantilever spring increases nonlinearly with the increase of grasping depth, which achieves the demand for different stiffnesses under different deformation envelopes. From the result of the effective length of the cantilever spring with the grasping depth, it can be seen that the effective length

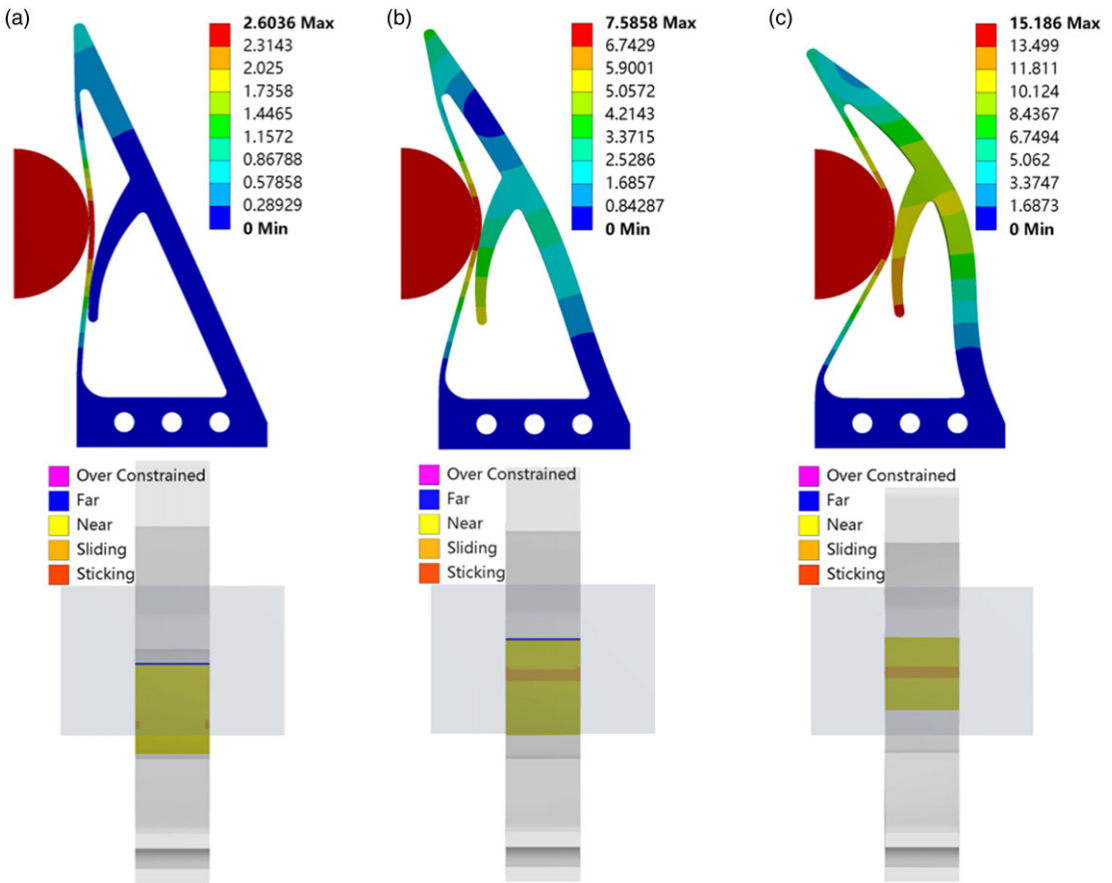


**Figure 9.** Finite element analysis results of the deformation of the cantilever spring-based variable stiffness finger (top) and the position of the contact surface between the front beam and the cantilever spring (bottom) at different grasping depths ( $x$ ): (a)  $x = 2.5$  mm; (b)  $x = 7.5$  mm; (c)  $x = 15$  mm.

decreases with the increase of the grasping depth at the grasping depth  $x = 2.5$  mm  $\sim$  11 mm; while at  $x = 11$  mm  $\sim$  15 mm, the effective length of the cantilever spring is almost unchanged, the reason is that at a larger grasping depth, the back beam of finger starts to produce larger deformation and drives the cantilever spring as a whole to move in the direction of the back-beam deformation, making the cantilever spring no longer continue to produce deformation.

### 4.3. Comparison of grasping performance

To demonstrate the improvements and advantages in the grasping performance of the finger designed based on the grasping force compensation method, a comparison was conducted under the same simulation settings outlined in Section 2.2 among the V-shaped finger, CSVS finger, and the commercial FRE finger, namely, model DHAS-80 from Festo as shown in Fig. 1(a). Figure 11 shows the FEA results for three types of fingers at a grasping depth of 15 mm, with specific numerical values compared as shown in Table 1.

Comparing the magnitude of the final total grasping force, the CSVS finger exhibits an improvement of approximately 7% over the V-shaped finger and an increase of approximately 59% over the FRE finger. Compared to the V-shape finger, the absolute value of the grasping force angle is reduced by approximately 5°, which is a reduction of about 74%, and the inflection point is advanced by approximately

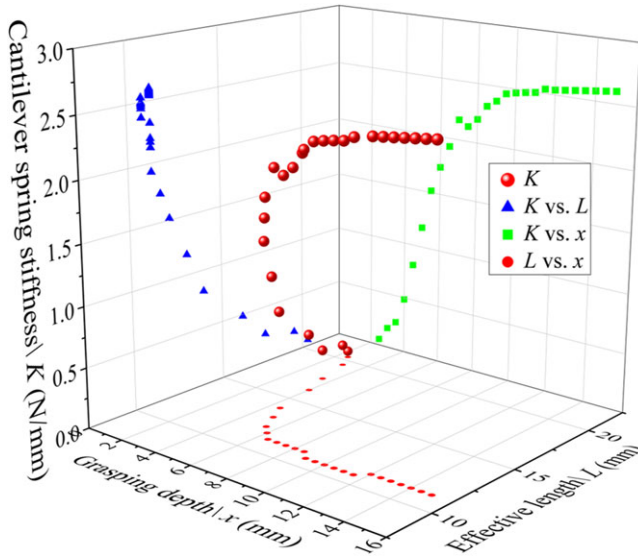


**Figure 10.** Relationship between the grasping depth ( $x$ ), the effective length ( $L$ ), and the stiffness ( $K$ ) of the cantilever spring.

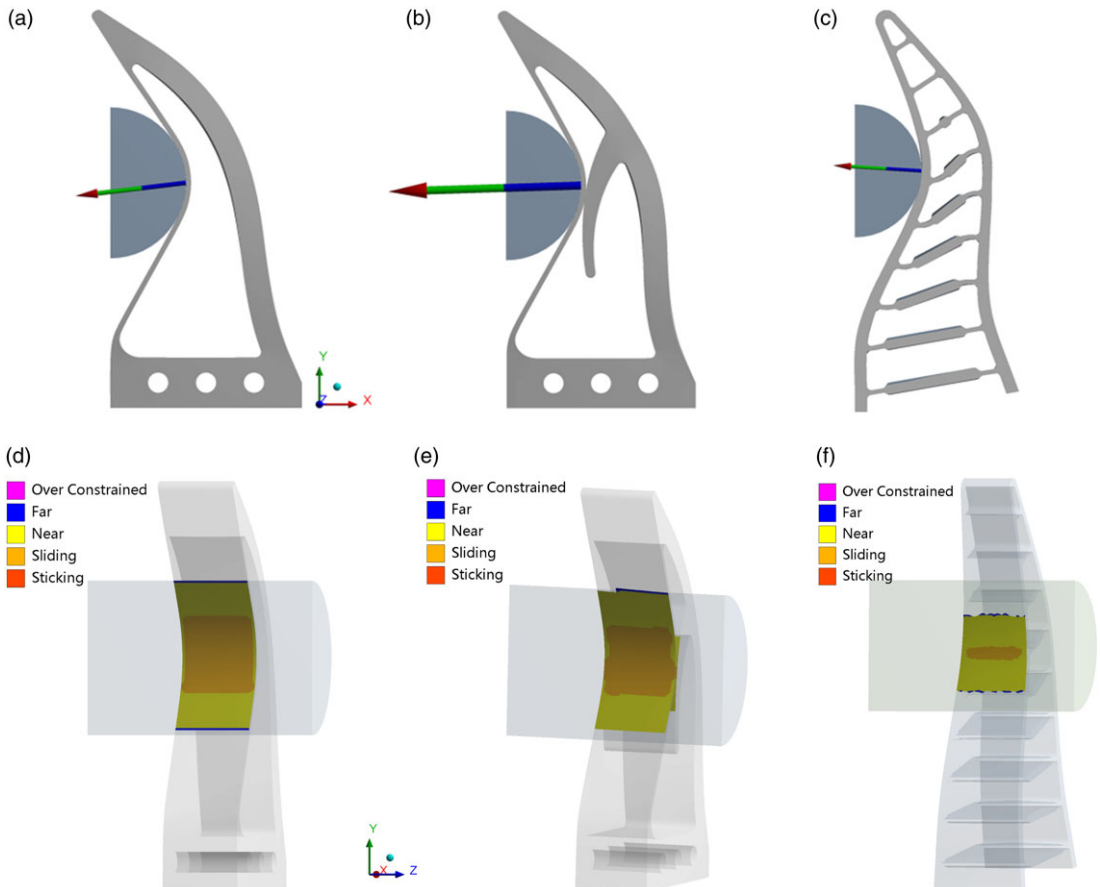
5 mm. Compared to the FRE finger, both the FRE finger and the CSVS finger have a certain magnitude of change in the grasping force angle in the pre-grasp stage, which is because of the adaptation of the finger to the shape of the grasped object. The final grasping force angle decreased by approximately 49%. Figures 11(a)–11(c) illustrate the direction of the final total grasping force for the three types of fingers. The smaller absolute value of the grasping force angle of the CSVS finger reduces the likelihood of the object sliding, while the positive grasping force angle of the FRE finger generates an outward pushing force on the object, increasing the possibility of the object detaching from the finger to some extent. Figures 11(d)–11(f), respectively, illustrate the contact status for the three types of fingers. According to the simulation results, the contact area of the CSVS finger is reduced by approximately 20 mm<sup>2</sup> compared to the V-shape finger, and the contact area ratio decreases by 1.62%. This is because the compensation effect of the cantilever spring increases the overall rigidity of the finger, leading to a reduction in the contact area. Although the FRE finger has a larger contact area of the front beam, its contact area differs significantly from the other two. The contact area between the CSVS finger and the grasped object is approximately 5 times that of the FRE finger, and the contact area ratio is about 6 times.

Figure 12(a) and (b), respectively, illustrate the grasping force responses and variations of grasping force angle with grasping depth for the three types of fingers. According to Section 4.2, it is evident that in the grasping depth range of 0 mm to 2.5 mm, the cantilever spring does not impact the finger’s grasping. Consequently, in Figs. 12(a) and (b), the variations in grasping force and grasping force angle for both the V-shaped finger and the CSVS finger are nearly identical. From Fig. 12(a), it can be also observed that the inflection point A occurs at the grasping depth of 4 mm because of the variable stiffness characteristic of the cantilever spring, which is approximately 33% earlier compared to the inflection point B of the V-shape finger. Furthermore, after point A, the grasping force of the CSVS finger gradually increases linearly with the grasping depth. The linear equation describing the relationship between the grasping force and the grasping depth in the post-grasp stage is obtained through the linear fitting of the grasping force data beyond point A and is as follows:

$$F = 1.01x - 3.876 \quad (4 \leq x \leq 15) \tag{10}$$

**Table I.** Comparison of grasping force, grasping force angle, and contact area ratio.

Finger type	$F_x$ (N)	$F_y$ (N)	$F_{tot}$ (N)	$\theta$ ( $^\circ$ )	$A_c$ (mm <sup>2</sup> )	$A_f$ (mm <sup>2</sup> )	$M$ (%)
V-shape finger	10.43	-1.25	10.50	-6.83	190.88	1260.50	15.10
CSVS finger	11.20	-0.36	11.21	-1.82	169.95	1260.50	13.48
FRE finger	7.04	0.46	7.05	3.54	35.14	1563.20	2.25



**Figure 11.** Finite element analysis result examples: (a) Final total grasping force by V-shape finger; (b) Final total grasping force by cantilever spring-based variable stiffness (CSVS) finger; (c) Final total grasping force by Fin Ray Effect finger DHAS-80 from festo; (d) Contact status of V-shape finger; (e) Contact status of CSVS finger; and (f) Contact status of FRE finger DHAS-80 from festo.

Where  $x$  is the grasping depth after the inflection point, and  $F$  is the grasping force at different grasp depths. The linear fitting coefficient ( $R^2$ ) of 0.999 7 is shown in the table in Fig. 12(a). From the fitting results, it can be observed that in the post-grasp stage, there is a high linear relationship between the grasping force and the grasp depth.

From Fig. 12(b), it can be observed that at point C, with a grasping depth of 2.5 mm, the cantilever spring begins compensating for the force of the front beam, ultimately resulting in the grasping force angle varying around  $-2^\circ$ . Compared to the inflection point D of the V-shaped finger, it is advanced by approximately 67%. Compared to the V-shape finger, the earlier grasping force response inflection point, greater grasping force, and smaller grasping force angle indicate the effectiveness of designing finger structure based on the grasping force compensation strategy for improving finger grasping performance.

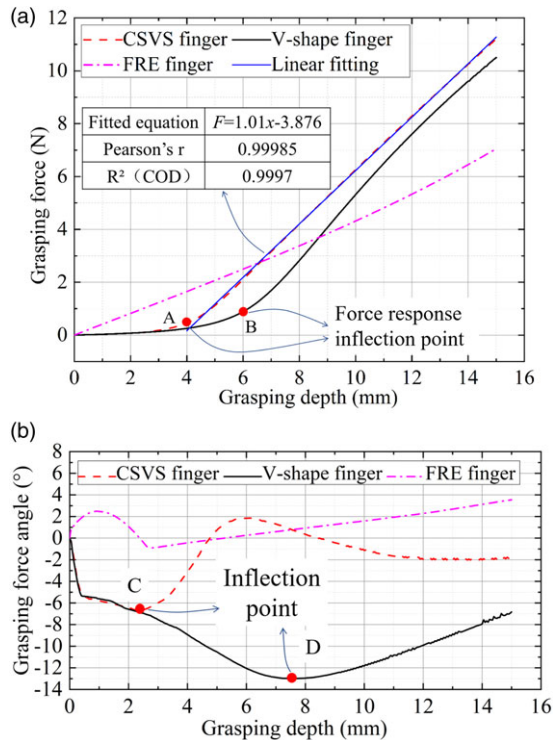


**Figure 12.** Comparison of the grasping performance among the V-shape finger, cantilever spring-based variable stiffness finger and Fin Ray Effect finger DHAS-80 from festo: (a) Grasping force; (b) Grasping force angle.

Meanwhile, compared to the FRE finger, the larger grasping force, smaller grasping force angle, and greater contact area ratio demonstrate the superiority of the grasping performance of the CSVs finger obtained through this strategy.

To further illustrate the significance and advantages of this design work, we compared the grasping performance of the CSVs finger with fingers proposed in the existing literature [13, 23]. However, due to the unknown specific design parameters of some fingers in the literature, variations in the materials used, and differences in the performance metrics employed to evaluate grasping performance, it is challenging to achieve a standardized comparison. Nevertheless, a common comparison with the FRE finger exists in these works and will be used as an intermediary to compare the grasping performance of each finger in terms of improvement rates. Rather than the fingertip deformation as the performance metric [3, 13], we consider the contact area ratio optimal for measuring the passive adaptability of fingers. Meanwhile, for comparison with other works, the simulations are also conducted to compare the fingertip deformation of the CSVs finger with the FRE finger.

Figure 13 shows the fingertip deformation of the fingers under comparison at a grasping depth of 15 mm, with the detailed displacement values and improvement rates listed in Table 2. It can be observed that the total displacement of the CSVs finger’s fingertip is 6.75% higher than that of Festo’s FRE finger. Although the increase in total displacement is slightly lower compared to the 15% reported in reference [13], as indicated by reference [3], when the grasped object moves to the finger along the positive  $x$ -axis, a smaller displacement of the fingertip along the positive  $x$ -axis and a larger displacement along the negative  $y$ -axis suggest that the finger absorbs more of the object’s displacement, indicating better adaptability of the finger. Compared to the FRE finger, the CSVs finger’s displacement along the negative  $x$ -axis, namely the opposite direction of the object displacement, is increased by 655%, which is more favorable for enveloping objects; the displacement along the negative  $x$ -axis toward the grasped

**Table II.** Comparison of the displacement of the fingertip of the cantilever spring-based variable stiffness (CSVS) and Fin Ray Effect (FRE) fingers.

Displacement of fingertip (mm)	FRE Finger	CSVS Finger	Improvement (%)
Total	5.63	6.01	6.75%
Along the x-axis	4.20	−2.35	655%
Along the y-axis	−3.95	−5.73	45.06%

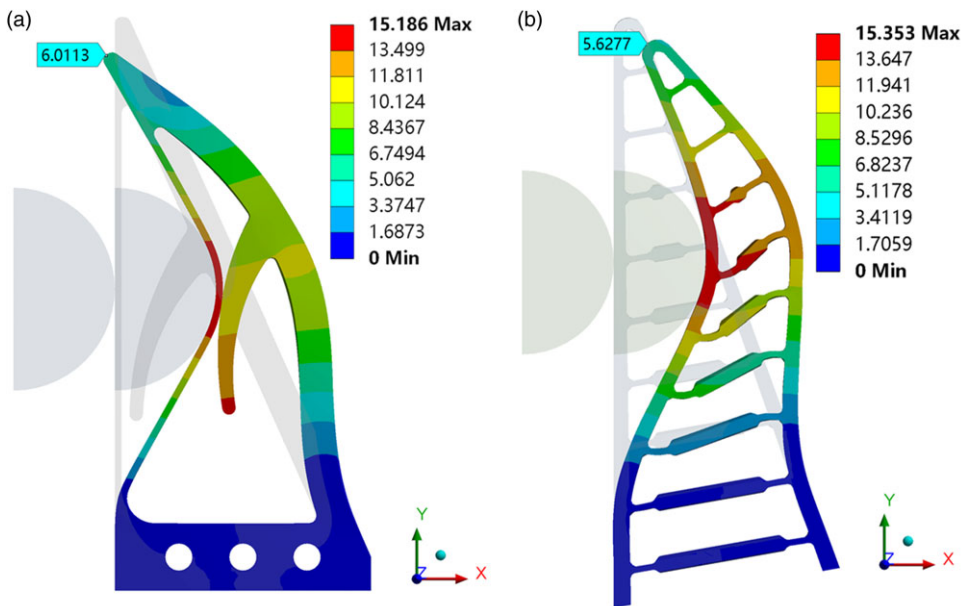


**Figure 13.** Displacement of the fingertip: (a) Cantilever spring-based variable stiffness finger; (b) Fin Ray Effect finger.

object is increased by 45.06% compared to the FRE finger. Regarding the magnitude of the grasping force, the CSVS finger’s grasping force is increased by 49% compared to that of the FRE finger. Compared to the improvement rate of 10.66% in reference [23], it has been increased by approximately 40%.

The above comparison results of the grasping performance show that compared to the V-shaped finger, the CSVS finger achieves the earlier grasping force response in the pre-grasp stage, the linear grasping force change, the larger grasping force, and the smaller grasping force angle in the post-grasp stage. This proves that the internal structure design based on grasping characteristics can effectively improve the finger’s performance. Compared to the FRE finger, the CSVS finger exhibits a higher grasping force, a smaller grasping force angle, a larger contact area ratio, and a larger displacement of fingertip. Compared to the fingers introduced in the literature [13, 23], the CSVS finger exhibits a larger displacement of fingertip and grasping force. Indeed, achieving the earlier inflection points and a smaller angle of grasping force during grasping can lead the finger to enter a stable grasping state sooner, reducing the likelihood of damaging the surface of delicate objects due to relative sliding. Moreover, the linear variation of grasping force with grasping depth allows for control over the grasping force by adjusting the grasping depth, addressing the challenge of predicting and controlling the grasping force in soft fingers. Additionally, the larger grasping force indicates that the fingers have stronger load-bearing capacity. The larger contact area ratio and displacement of the fingertip suggest that the fingers have better adaptability.

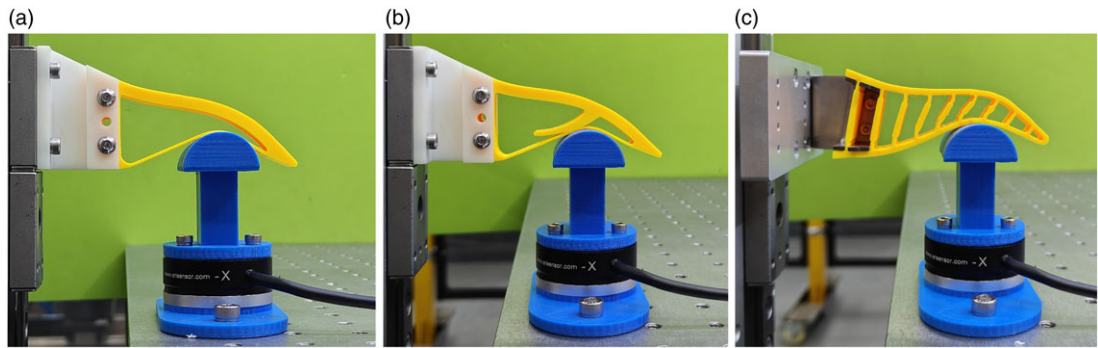


**Figure 14.** Test setup for the grasping force: (a) V-shape finger; (b) cantilever spring-based variable stiffness finger; (c) Fin Ray Effect finger.

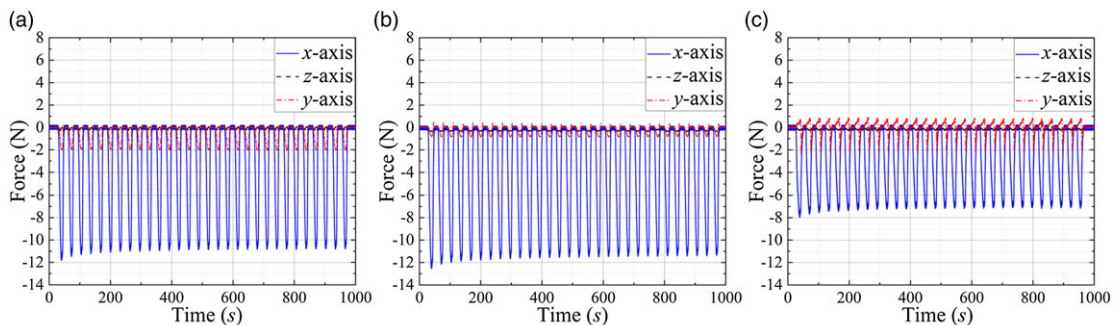


**Figure 15.** Records of the grasping force measurements in three axes: (a) V-shape finger; (b) Cantilever spring-based variable stiffness finger; and (c) Fin Ray Effect finger.

## 5. Experiments

To evaluate the grasping performance and further validate the accuracy of the FEA model of the CSVS finger, the grasping force tests and grasping tests of various target objects were conducted on a FANUC robot with model number M-10iD12 as the experimental platform.

### 5.1. Grasping force tests

To validate the accuracy of the FEA model, the grasping force tests were conducted with the device (shown in Fig. 14). This device was used to measure the variation of grasping force with respect to the grasping depth during the grasping process of the soft finger. All fingers were 3D-printed in the same elastic material (NinjaFlex by Ninjatek) and mounted on an industrial parallel gripper. The FRE finger DHAS-80 from Festo uses a tilted adapter allowing the finger's front beams to be perpendicular to the base as well as the grasping direction, while the V-shaped finger and CSVS fingers proposed in this study already consider the grasping motion and do not need such adjustment in angles. The sensor used in the experiment is the SRI M3703C 6-axis force/torque sensor. It was securely fixed to the testing platform through a base. Above the sensor, a simulated cylindrical object, with the same diameter as the object used in the FEA, was fixed. Both the rigid base and cylindrical object were 3D printed using the Acrylonitrile Butadiene Styrene (ABS) material. The contact position between the soft finger and the object is adjusted to match the position used in the FEA and moved downward along the vertical direction for 15 mm.

In each series of measurements, 30 vertical compressions were performed to average the grasping force. The test results for grasping force are plotted in Fig. 15, while the corresponding statistical data



**Table III.** Test results of the grasping force and grasping force angle of V-shape finger.

Variables	Mean	Median	Minimum	Maximum	Standard deviation	Units
$F_x$	10.97	10.88	10.77	11.82	0.23	N
$F_y$	2.01	2.03	2.05	1.94	0.03	N
$F_{tot}$	11.15	11.07	10.96	11.99	0.22	N
$\theta$	-10.39	-10.54	-10.39	-9.65	0.33	°

**Table IV.** Test results of the grasping force and grasping force angle of cantilever spring-based variable stiffness finger.

Variables	Mean	Median	Minimum	Maximum	Standard deviation	Units
$F_x$	11.61	11.53	11.37	12.51	0.26	N
$F_y$	0.83	0.84	0.79	0.85	0.02	N
$F_{tot}$	11.64	11.56	11.40	12.56	0.26	N
$\theta$	-4.08	-4.02	-4.23	-3.60	0.12	°

**Table V.** Test results of the grasping force and grasping force angle of Fin Ray Effect finger.

Variables	Mean	Median	Minimum	Maximum	Standard deviation	Units
$F_x$	7.26	7.18	7.10	7.97	0.20	N
$F_y$	0.82	0.82	0.71	0.91	0.04	N
$F_{tot}$	7.31	7.22	7.14	8.00	0.19	N
$\theta$	6.43	6.46	5.09	7.12	0.35	°

for the  $x$ - and  $y$ -axes, as well as the calculated total grasping force and grasping force angle, are listed in Tables 3, 4, and 5, respectively.

The grasping force along the  $z$ -axis fluctuates within a range of 0.5 N. In comparison to the grasping force of the simulated results for the  $z$ -axis, this fluctuation falls within the allowable range of measurement error. The grasping forces and angles obtained from the FEA in Table 1 can be compared with the test results in Tables 3, 4, and 5, as listed in Table 6. Clearly, for these three different structures, FEA accurately predicted the test results for the grasping force of the  $x$ -axis. Considering the  $y$ -axis grasping force, it is slightly larger than the FEA results but still within 1 N, ultimately resulting in a grasping force angle slightly larger than the FEA results. This difference in grasping force may be attributed to discrepancies in the height of the contact point and the finger displacement between the actual experiment and the FEA. In addition, It should be noted that, due to the absence of soft sensors in the current market capable of accurately measuring the contact area, experimental validation of the contact area ratio was not conducted in this study. Nevertheless, the validation results of grasping force and grasping force angle are sufficient to affirm the accuracy of the FEA model. This also emphasizes the necessity of employing FEA for evaluating the contact area ratio.

## 5.2. Generalization to object shape and contact point

To further evaluate the grasping performance of the CSVS finger, the simulation experiments were conducted in two scenarios: grasping cylinders of different diameters ( $D = 20$  mm, 30 mm, 40 mm, 50 mm, and 60 mm) at the same contact point height ( $H = 45$  mm) and grasping cylinders of the same diameter ( $D = 30$  mm) at different contact point heights ( $H = 35$  mm, 45 mm, 55 mm, 65 mm, and 75 mm). These

**Table VI.** Comparison of the finite element analysis (FEA) and test result (separated by colon).

Variables	V-shape (FEA : Test)	CSVS finger (FEA : Test)	FRE finger (FEA : Test)	Units
$F_x$	10.43 : 10.97	11.20 : 11.61	7.04 : 7.26	N
$F_y$	1.25 : 2.01	0.36 : 0.83	0.46 : 0.82	N
$F_{tot}$	10.50 : 11.15	11.21 : 11.64	7.05 : 7.31	N
$\theta$	-6.83 : -10.39	-1.82 : -4.08	3.54 : 6.43	°

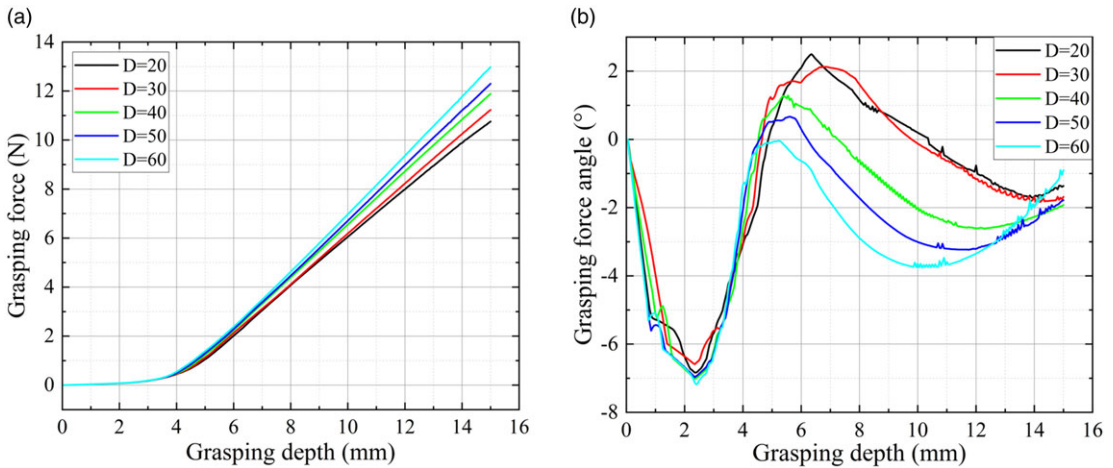
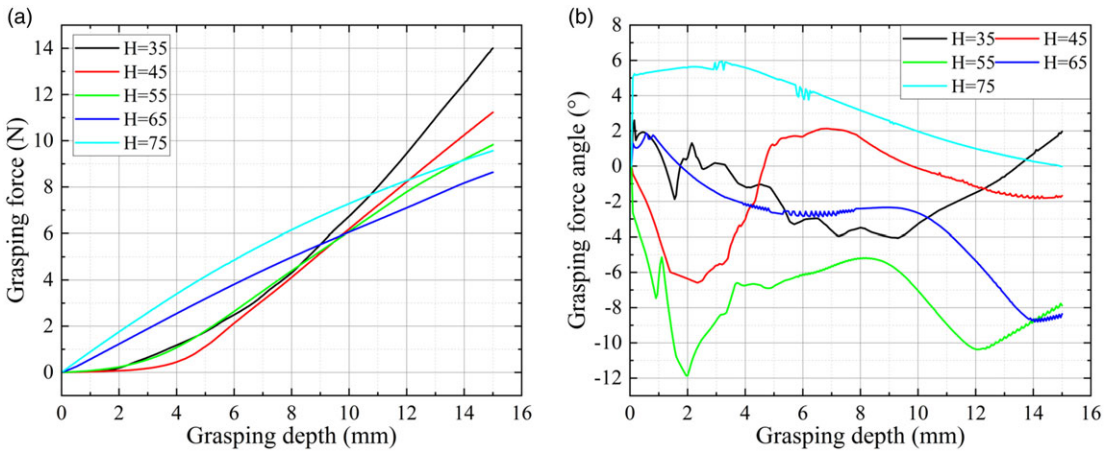


**Figure 16.** Grasping performance of cantilever spring-based variable stiffness finger for grasping cylindrical objects of different diameters at the same height of the contact point ( $H = 45$  mm): (a) Grasping force response; (b) Grasping force angle.

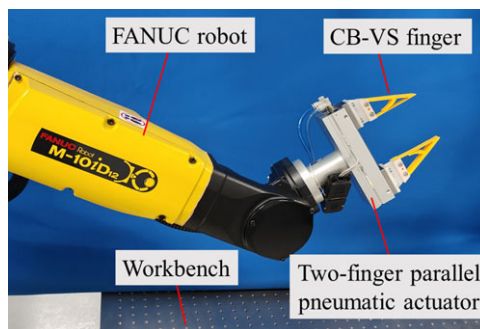
experiments aimed to explore the impact of changes in the object shape and the height of the contact point on the grasping performance. The simulation settings were based on Section 2.2.

Figure 16 compares the grasping force response and the variation of the grasping force angle when grasping cylinders of different diameters at the contact point height  $H = 45$  mm. As depicted in Fig. 16(a), it is observed that, when grasping cylinders of various diameters, there is a consistent grasping force response in the pre-grasp stage, with the cantilever spring compensating for the forces at  $x = 4$  mm. In the post-grasp stage, the grasping force response increases with the diameter of the grasped object. From Fig. 16(b), it is evident that there is also a consistent variation of the grasping force angle in the pre-grasp stage, with the cantilever spring providing compensation at  $x = 2.5$  mm. In the post-grasp stage, the grasping force angle for all series ultimately remains within the range of  $0^\circ$  to  $-2^\circ$ .

Figure 17 compares the grasping force response and the variation of the grasping force angle when grasping cylinders with a diameter of 30 mm at different contact point heights. As shown in Fig. 17(a), with the decrease in contact point height, the inflection point in the grasping force response occurs earlier, resulting in a higher final grasping force. This is attributed to the arc-shaped structure of the cantilever spring, which, with a lower contact point height, provides force compensation earlier during grasping at the same depth. As a result, the cantilever spring undergoes greater deformation, leading to a higher grasping force. It should be noted that when  $H = 55$  mm  $\sim$  75 mm, the cantilever spring almost does not provide compensation, and the finger primarily relies on the deformation of the back beam to generate the grasping force. The grasping force responses at these contact point heights are similar to the grasping force response of the FRE finger shown in Fig. 12(a). Furthermore, upon reaching a certain height, such as  $H = 75$  mm, the corresponding grasping force response is greater than that at  $H = 65$  mm. This is because, at this position, the finger adopts a pinching form at the fingertip, where the front beam does not adapt to the shape of the grasped object. Instead, it inhibits the deformation of the back beam,



**Figure 17.** Grasping performance of cantilever spring-based variable stiffness finger for grasping a cylindrical object of the same diameter ( $D = 30$  mm) at different heights of contact points: (a) Grasping force response; (b) Grasping force angle.



**Figure 18.** Test platform for grasping various objects.

consequently increasing the stiffness of the finger to pinch the object firmly. From Fig. 17(b), it can be observed that the grasping force angles generated at the contact point heights  $H = 55$  mm and 65 mm are relatively large. This phenomenon arises due to the limited compensation effect of the cantilever spring on finger grasping at these heights, whereas the final grasping force angles at other contact heights remain within the range of  $\pm 2^\circ$ .

From the above analysis, it is evident that changing the size of the grasped object does not alter the grasping performance of the finger. However, varying the contact point height results in changes in grasping performance due to the structural characteristics of the internal cantilever spring within the finger. Typically, optimal grasping poses are selected during object manipulation, mitigating the impact of height variations. Leveraging machine vision for control of grasping height can address this issue. Additionally, this insight suggests that optimizing the finger's grasping performance under variations in contact point height could be achieved by increasing the number of cantilever spring structural units.

### 5.3. Grasping tests of various target objects

To test the adaptability of the CSVS finger, the grasping tests of various target objects were conducted using the FANUC robot test platform shown in Fig. 18. The experiments are performed with pneumatic actuators at a pressure of 0.2 MPa. As shown in Fig. 19, the experiments involved grasping objects of various shapes and weights commonly found in daily life, such as eggs, apples, mouse, cups, and so on.

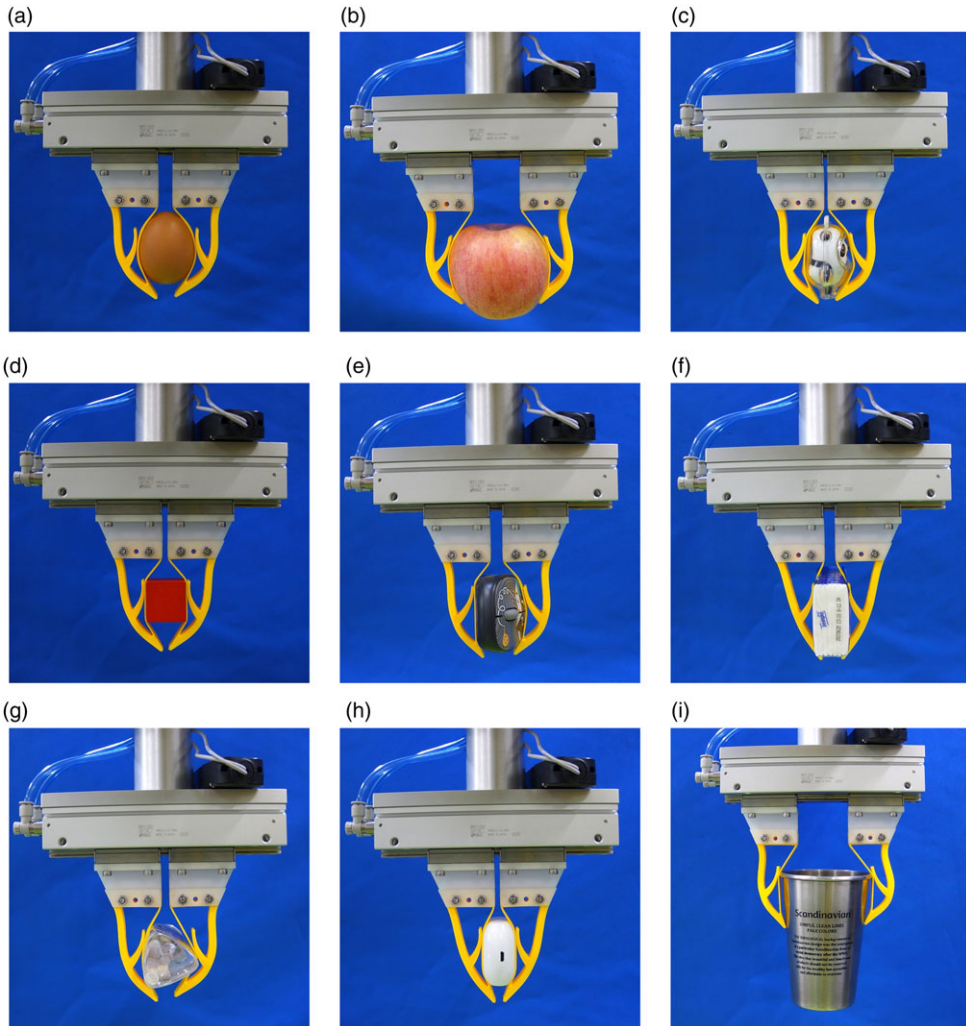


**Figure 19.** Grasping tests of various target objects: (a) Egg; (b) Apple; (c) Doll; (d) Square block; (e) Mouse; (f) Tissue paper; (g) Candy box; (h) Headphone box; and (i) Cup.

The grasping results from Fig. 19(a) and (f) indicate that the soft finger can reliably grasp fragile and deformable objects. From the grasping results shown in Fig. 19(a), (b), (d), and (h), when grasping symmetrically shaped and regularly surfaced objects, the soft finger can perfectly adapt to the shape of the grasped object. The contact area between the soft finger's front beam and the grasped object is maximized. Even when grasping a heavier object as shown in Fig. 19(b), the finger still exhibits good adaptability and stable grasping, indicating that the finger not only possesses good adaptability but also maintains good rigidity under the compensatory effect of the cantilever spring. The grasping results from Fig. 19(c) and (e) reveal that when grasping asymmetrically shaped objects, the front beams of the two fingers can adaptively deform according to the surfaces they contact. Additionally, from Fig. 19(c), it can be observed that the thinner front beam can completely envelop the protruding part of the grasped object. Finally, from the grasping results shown in Fig. 19(g) and (i), when grasping objects with edges, the front beam adapts to the shape of the grasped object as much as possible, effectively demonstrating the compensatory effect of the cantilever beam structure. The results of numerous experiments have shown that the soft robotic hand with the CSVS fingers can perform adaptive, nondestructive,

and stable grasping according to the shape of the object when grasping objects of different shapes and sizes.

## 6. Conclusion

In this paper, our focus is to propose a design method for the internal structure based on the required grasping performance characteristics of the soft fingers. Specifically, the proposed V-shaped finger of the fundamental architecture was evaluated using three performance metrics: grasping force response, grasping force angle, and contact area ratio. Issues including delayed grasping force response in the pre-grasp stage, nonlinear grasping force change, and large grasping force angle in the post-grasp stage were addressed by introducing a design method that compensates for the grasping force of the V-shaped finger using the characteristics of the CSVS mechanism. Unlike previous studies in which minor changes were made to the internal structure, a cantilever spring with CSVS mechanism characteristics was selectively added to the interior of the V-shaped finger, forming the CSVS soft finger. The structure was then optimized to achieve earlier grasping force responses in the pre-grasp stage, larger and more linearly changing grasping force in the post-grasp stage, and smaller grasping force angle. Based on FEA, the variable stiffness characteristics of the CSVS mechanism are verified, and comparison with V-shaped and Festo's FRE fingers demonstrated the superior grasping characteristics of our proposed CSVS finger. Experimental validation using 3D-printed soft fingers confirmed the accuracy of the FEA model. In generalization experiments with various object shapes and contact points, the finger exhibited consistent grasping characteristics. Additionally, grasping tests on various target objects demonstrated the excellent adaptability of the designed fingers. However, it was observed that changes in contact point height significantly affected the grasping force angle, which could be addressed through machine vision to determine the optimal grasping position. In future work, the impact of contact height on grasping performance will be addressed by adding multiple cantilever spring structural units within the finger to compensate for force at different contact point heights. Overall, this work provides a novel perspective for the optimization and design of soft robotic grippers.

**Author contributions.** Xiaowei Shan proposed the design methodology and the structures. Litao Xu optimized the structures and conducted the experiments. Xuefei Li assisted with the experiments. Xiaowei Shan and Litao Xu wrote this article.

**Financial support.** This work was supported by the Beijing University of Civil Engineering and Architecture (BUCEA) Project (grant number 06082721005) and the BUCEA Post Graduate Innovation Project (grant number PG2023142).

**Competing interests.** The authors declare that no conflicts of interest exist.

**Ethical approval.** None.

## References

- [1] L. Birglen and T. Schlicht, "A statistical review of industrial robotic grippers," *Robot Comput Integr Manuf* **49**, 88–97 (2018).
- [2] M. Dong and J. Zhang, "A review of robotic grasp detection technology," *Robotica* **41**(12), 3846–3885 (2023).
- [3] K. Elgeneidy, A. Fansa, I. Hussain and K. Goher, "Structural Optimization of Adaptive Soft Fin Ray Fingers with Variable Stiffening Capability," *In: 3rd IEEE International Conference on Soft Robotics (RoboSoft)*, (2020) pp. 779–784.
- [4] Q. M. Marwan, S. C. Chua and L. C. Kwek, "Comprehensive review on reaching and grasping of objects in robotics," *Robotica* **39**(10), 1849–1882 (2021).
- [5] FESTO, MultiChoiceGripper. (2023). [https://www.festo.com/net/SupportPortal/Files/333986/Festo\\_MultiChoiceGripper\\_en.pdf](https://www.festo.com/net/SupportPortal/Files/333986/Festo_MultiChoiceGripper_en.pdf).
- [6] J. Shintake, V. Cacucciolo, D. Floreano and H. Shea, "Soft robotic grippers," *Adv Mater* **30**(29), 1707035 (2018).
- [7] J. Hu, L. Liang and B. Zeng, "Design, modeling, and testing of a soft actuator with variable stiffness using granular jamming," *Robotica* **40**(7), 2468–2484 (2022).

- [8] V. Ferrandy, Indrawanto, F. Ferryanto, A. Sugiharto, E. Franco, A. Garriga-Casanovas, A. I. Mahyuddin, F. Rodriguez y Baena, S. Mihradi and V. Virdyawan, "Modeling of a two-degree-of-freedom fiber-reinforced soft pneumatic actuator," *Robotica* **41**(12), 3608–3626 (2023).
- [9] W. Xiao, C. Liu, D. Hu, G. Yang and X. Han, "Soft robotic surface enhances the grasping adaptability and reliability of pneumatic grippers," *Int J Mech Sci* **219**, 107094 (2022).
- [10] R. Chen, R. Song, Z. Zhang, L. Bai, F. Liu, P. Jiang, D. Sindensberger, G. J. Monkman and J. Guo, "Bio-inspired shape-adaptive soft robotic grippers augmented with electroadhesion functionality," *Soft Robot* **6**(6), 701–712 (2019).
- [11] R. Chen, Z. Zhang, J. Guo, F. Liu, J. Leng and J. Rossiter, "Variable stiffness electroadhesion and compliant electroadhesive grippers," *Soft Robot* **9**(6), 1074–1082 (2022).
- [12] D.-S. Choi, T.-H. Kim, S.-H. Lee, C. Pang, J. W. Bae and S.-Y. Kim, "Beyond human hand: Shape-adaptive and reversible magnetorheological elastomer-based robot gripper skin," *ACS Appl Mater Interf* **12**(39), 44147–44155 (2020).
- [13] W. Crooks, G. Vukasin, M. O'Sullivan, W. Messner and C. Rogers, "Fin ray® effect inspired soft robotic gripper: From the roboSoft grand challenge toward optimization," *Front Robot AI* **3**, 70–78 (2016).
- [14] FESTO, Adaptive gripper fingers DHAS, (2023). <https://www.festo.com/media/pim/049/D15000100122049.PDF>.
- [15] X. Shan and L. Birglen, "Bistable stopper design and force prediction for precision and power grasps of soft robotic fingers for industrial manipulation," *J Mech Design* **146**(4), 045001 (2024).
- [16] N. Mouazé and L. Birglen, "Bistable compliant underactuated gripper for the gentle grasp of soft objects," *Mech Mach Theory* **170**, 104676 (2022).
- [17] C.-H. Liu, C.-H. Chiu, M.-C. Hsu, Y. Chen and Y.-P. Chiang, "Topology and size-shape optimization of an adaptive compliant gripper with high mechanical advantage for grasping irregular objects," *Robotica* **37**(8), 1383–1400 (2019).
- [18] C.-H. Liu, M.-C. Hsu, T.-L. Chen and Y. Chen, "Optimal design of a compliant constant-force mechanism to deliver a nearly constant output force over a range of input displacements," *Soft Robot* **7**(6), 758–769 (2020).
- [19] J. Y. Lee, Y. S. Seo, C. Park, J. S. Koh, U. Kim, J. Park, H. Rodrigue, B. Kim and S. H. Song, "Shape-adaptive universal soft parallel gripper for delicate grasping using a stiffness-variable composite structure," *IEEE Trans Ind Electron* **68**(12), 12441–12451 (2021).
- [20] L. Li, F. Xie, T. Wang, G. Wang, Y. Tian, T. Jin and Q. Zhang, "Stiffness-tunable soft gripper with soft-rigid hybrid actuation for versatile manipulations," *Soft Robot* **9**(6), 1108–1119 (2022).
- [21] X. Shan and L. Birglen, "Modeling and analysis of soft robotic fingers using the fin ray effect," *Int J Robot Res* **39**(14), 1686–1705 (2020).
- [22] C. Armanini, I. Hussain, M. Z. Iqbal, D. Gan, D. Praticchizzo and F. Renda, "Discrete cosserat approach for closed-chain soft robots: Application to the fin-ray finger," *IEEE Trans Robot* **37**(6), 2083–2098 (2021).
- [23] K. Elgeneidy, P. Lightbody, S. Pearson and G. Neumann, "Characterising 3D-Printed Soft Fin Ray Robotic Fingers with Layer Jamming Capability for Delicate Grasping," *In: 2019 2nd IEEE International Conference on Soft Robotics (RoboSoft)*, (2019) pp. 143–148.
- [24] C. I. Basson, G. Bright and A. J. Walker, "Analysis of Flexible End-Effector for Geometric Conformity in Reconfigurable Assembly Systems: Testing Geometric Structure of Grasping Mechanism for Object Adaptability," *In: 2017 Pattern Recognition Association of South Africa and Robotics and Mechatronics (PRASA-RobMech)*, (2017) pp. 92–97.
- [25] C. I. Basson and G. Bright, "Geometric Conformity Study of a Fin Ray Gripper Utilizing Active Haptic Control," *In: 2019 IEEE 15th International Conference on Control and Automation (ICCA)*, (2019) pp. 713–718.
- [26] L. Y. Lee, S. G. Nurzaman and C. P. Tan, "Design and Analysis of a Gripper with Interchangeable Soft Fingers for Ungrounded Mobile Robots," *In: 2019 IEEE International Conference on Cybernetics and Intelligent Systems (CIS) and IEEE Conference on Robotics, Automation and Mechatronics (RAM)*, (2019) pp. 221–226.
- [27] J. H. Shin, J. G. Park, D. I. Kim and H. S. Yoon, "A universal soft gripper with the optimized fin ray finger," *Int J Pr Eng Man-Gt* **8**, 889–899 (2021).
- [28] J. Yao, Y. Fang and L. Li, "Research on effects of different internal structures on the grasping performance of fin ray soft grippers," *Robotica* **41**(6), 1762–1777 (2023).
- [29] R. K. Hota and C. S. Kumar, "Effect of design parameters on strong and immobilizing grasps with an underactuated robotic hand," *Robotica* **40**(11), 3769–3785 (2022).
- [30] A. Bicchi, "Hands for dexterous manipulation and robust grasping: A difficult road toward simplicity," *IEEE Trans Robot Automat* **16**(6), 652–662 (2000).
- [31] G. A. Kragten and J. L. Herder, "The ability of underactuated hands to grasp and hold objects," *Mech Mach Theory* **45**(3), 408–425 (2010).
- [32] J. Suder, Z. Bobovský, J. Mlotek, M. Vocetka, P. Oščádal and Z. Zeman, "Structural optimization method of a finRay finger for the best wrapping of object," *Appl Sci* **11**(9), 3858 (2021).
- [33] L. Kniese, "Load carrying element with flexible outer skin," European Patent Office EP1040999A2, (1999).
- [34] J. Falco, K. Van Wyk and E. Messina, "Performance Metrics and Test Methods for Robotic Hands," *DRAFT NIST Spec Public* **1227**, 2–2 (2018).
- [35] D. De Barrie, M. Pandya, H. Pandya, M. Hanheide and K. Elgeneidy, "A deep learning method for vision based force prediction of a soft fin ray gripper using simulation data," *Front Robot AI* **8**, 631371 (2021).
- [36] T. Reppel and K. Weinberg, "Experimental determination of elastic and rupture properties of printed ninjaflex," *Tech Mech* **38**(1), 104–112 (2018).
- [37] S. H. Yeo, G. Yang and W. B. Lim, "Design and analysis of cable-driven manipulators with variable stiffness," *Mech Mach Theory* **69**, 230–244 (2013).

- [38] Y.-S. Wu and C.-C. Lan, “Linear variable-stiffness mechanisms based on preloaded curved beams,” *J Mech Design* **136**(12), 122302 (2014).
- [39] Z. Xie, L. Qiu and D. Yang, “Analysis of a novel variable stiffness filleted leaf hinge,” *Mech Mach Theory* **144**, 103673 (2020).

---

**Cite this article:** X. Shan, L. Xu and X. Li (2024). “A variable stiffness design method for soft robotic fingers based on grasping force compensation and linearization”, *Robotica* **42**, 2061–2083. <https://doi.org/10.1017/S026357472400081X>